REVIEW

Synthesis of needle-like aragonite using carbonation method: A review

Hiroshi SAKUMA*, Shigeru SUEHARA*, Hidenobu NAKAO**, Je-Deok KIM* and Kenji TAMURA*

*Environmental Circulation Composite Materials Group, National Institute for Materials Science, Tsukuba 305-0044, Japan
**Hydrogen Related Materials Group, National Institute for Materials Science, Tsukuba 305-0044, Japan

The environmental problems caused by CO_2 emissions endanger human lives. Under these circumstances, carbon dioxide capture, utilization, and storage (CCUS) is likely to reduce CO_2 gas emissions with economic advantages. An application of CCUS is the reinforcement of mechanically weak bio-based composite plastics. Needle-like calcium carbonate crystals can potentially reinforce weak plastics. Moreover, the synthesis of calcium carbonate via carbonation can reduce CO_2 emissions. Here, we review the development of synthetic methods for needle-like aragonite (which is a polymorph of calcium carbonate crystals) using a gaseous CO_2 for further development of efficient synthetic conditions and precise control of morphology. Various factors influencing the synthesis of aragonite have been discussed. These include the temperature; degree of supersaturation of $CaCO_3$; pH; additives; and external stimuli such as high gravity, sound waves, and microbubbles. The estimated elastic moduli of aragonite were anisotropic depending on the crystal direction. This indicated the importance of controlling the long-axis direction of aragonite as a novel reinforcement material.

Keywords: Aragonite, Aspect ratio, Elastic constants, CO_2

INTRODUCTION

An increase in atmospheric carbon dioxide concentration can cause severe environmental transitions on Earth's surface through the greenhouse effect. Carbon dioxide capture and storage (CCS) has been studied to store CO_2 underground. However, this process does not generate economic advantages because the recovered CO_2 is only waste. Carbon dioxide capture, utilization, and storage (CCUS) is likely to have an economic impact by utilizing CO_2 gas (Woodall et al., 2019). Currently, CO_2 gas is used mainly to improve oil recovery. However, this process does not contribute to CO_2 reduction. Therefore, there is a need for effective utilization methods.

One of the utilization methods is the use of precipitated calcium carbonate (PCC) from CO_2 gas as a reinforcing agent filler in the plastic, rubber, and paper industries (Fig. 1) (Hu et al., 2009; Jimoh et al., 2018; Liendo et al., 2022; Zhong et al., 2024b). Bio-based polymers are likely to replace petroleum-based polymers in common plastics to reduce the CO_2 emissions during oil mining.

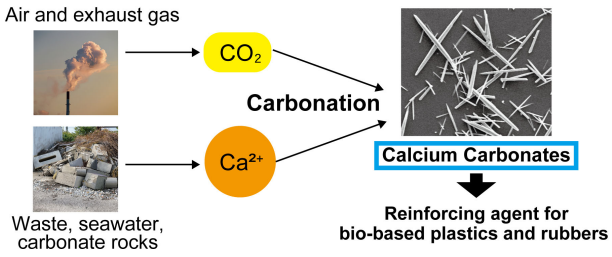

Figure 1. Utilization of CO_2 gas as a reinforcing agent for bio-base plastics and rubbers.

A drawback of bio-based plastics is their low mechanical strength. Composite materials are generally used for plastics by adding reinforcement materials to polymers. If the PCC crystal made from CO_2 gas can be used as a reinforcement material, CO_2 gas may be utilized effectively. PCC is light, non-hazardous, and can be recycled conveniently with acids. Acids have the capacity to dissolve calcium carbonates, resulting in the emission of CO_2 gas. In the recycling process, the CO_2 gas can be utilized once more to synthesize calcium carbonate particles.

PCC has been applied for reinforcing plastics and can improve the impact strength of polypropylene (PP) (Lin et al., 2010; Moritomi et al., 2010). However, the

doi:10.2465/jmps.240819
H. Sakuma, SAKUMA.Hiroshi@nims.go.jp Corresponding author

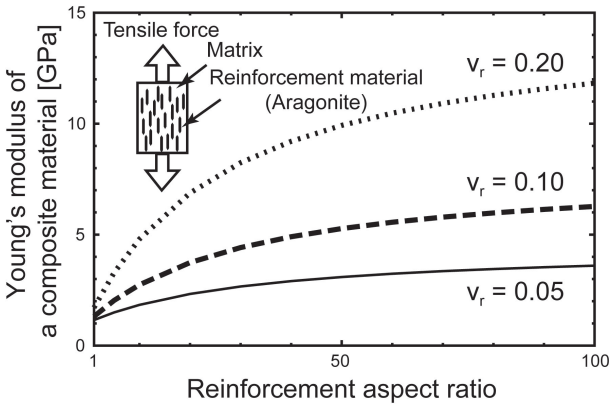

Figure 2. Young's modulus of a composite material calculated using the Halpin–Tsai model. Here, the Young's moduli of matrix and aragonite reinforcement are assumed as 1 GPa and 70 GPa, respectively. The results for three volume fractions of reinforcement material (v_r) are plotted.

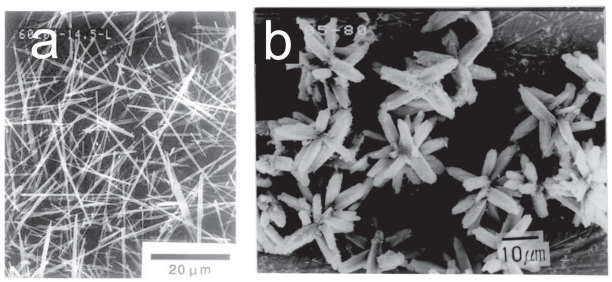

Figure 3. Morphology of (a) needle-like (Ota et al., 1995) and (b) branched (Ahn et al., 2004) aragonite synthesized by the carbonation method. Reprinted with permission from Wiley.

flexural modulus is not improved significantly compared with conventional fillers such as glass fiber and talc (Moritomi et al., 2010). One of the reasons for the low flexural modulus may be the low aspect ratio of calcite (a polymorph of calcium carbonate), although the properties of composites depend on various factors such as the degree of dispersion, crystal size, and interfacial interaction between polymers and crystals. Theoretically, as shown by the Halpin–Tsai model (Halpin, 1969; Halpin and Kardos, 1976; Mallick, 2007), an increase in the aspect ratio of the fillers improves the flexural modulus of the composites. The Young's modulus of an ideal composite estimated by the Halpin–Tsai model increases with increases in the aspect ratio of fiber reinforcement and volume fraction of reinforcement (v_r), as shown in Figure 2. The Young's moduli of the matrix and reinforcement were assumed to be 1 GPa and 70 GPa, respectively. In fact, an increase in the aspect ratio of glass fibers improves the Young's modulus of epoxy in their composites (Wakashima, 1976). These studies indicated that controlling the morphology of PCC is critical for improving the mechanical properties of composite materials.

The morphology of the PCC varies depending on the polymorphs of calcite, aragonite, and vaterite. Calcite is the most stable polymorph under ambient conditions. Its shape is mainly rhombohedral or spindle-like (scalenohedron). Aragonite has a denser structure than calcite and is metastable at room temperature and 1 atm pressure. However, it can be synthesized by increasing the temperature of the starting solution and/or the presence of additives. The morphology of aragonite is characterized by needle-like and branched forms, as shown in Figure 3 (Ota et al., 1995; Ahn et al., 2004). Vaterite is metastable and exhibits spherical and plate-like shapes. Owing to the large aspect ratio of the fillers, which improves the mechanical properties of composite materials, aragonite is the best candidate among these three polymorphs. The attempt to apply columnar calcium carbonates as a filler of PP has improved the tensile and flexural strength and these moduli (Jing et al., 2018). The mechanically tough and shock-resistance crystal phase of PP (β phase) can be formed using aragonite as a nucleating agent (Guan et al., 2013).

Aragonite synthesis has a long history, and various conditions have been tested to find the conditions for pure aragonite synthesis. There are several ways to obtain aragonite, such as metathesis reaction, urea hydrolysis, and biomineralization; however, the carbonation method directly using gaseous CO_2 has become the primary method recently due to the need for carbon reduction. This review provides the synthesis by the carbonation method to control its morphology and aspect ratio of aragonite. The factors likely to influence the aspect ratio, such as the temperature, Ca and CO_2 concentrations, pH, additives (Mg, NH_3, etc.), and external stimuli, are discussed for the further development of aragonite synthesis.

ARAGONITE SYNTHESIS USING A CARBONATION METHOD

The available reports on the synthesis of aragonite using carbonation methods are listed in Table 1. The synthesis of calcium carbonate from CO_2 gas can be classified based on the source of Ca. One is the use of lime (CaO) and slaked lime [$Ca(OH)_2$], and the other is the use of Ca salts. Seawater, slag, and concrete waste should be considered as potential sources of Ca (Ho and Iizuka, 2023; Shen et al., 2023; Zhong et al., 2024a). However, these materials contain various ions, minerals, and organic matter; therefore, their complicated composition is beyond the scope of this paper when it comes to finding optimal conditions for needle-like aragonite synthesis. Here we focus on simple Ca sources such as lime and Ca salts.

Table 1. Experimental conditions of aragonite synthesis using carbonation method, arranged in chronological order of publication

Morphology	Aspect ratio	Ca source	Additives, special techniques	CO_2 feed rate (CO_2 gas, L/min/Solution, L)	T (°C)	Reference
Needle like	?	$Ca(OH)_2$	Sucrose	~ 0.39	60–90	Bennett and Gardiner, 1967
Columnar	~ 10	$Ca(OH)_2$	Three-step reactions	0.02–15	1: 5–20 2: 7–25 3: >45	Murakami et al., 1977
Needle like	~ 10	$Ca(OH)_2$	MEA, HNO_3	0.0008–0.04	>60	Langelin et al., 1984
Needle like	~ 20	$Ca(OH)_2$	Sucrose	1.0	>70	Ota et al., 1986
Needle like	~ 20	$CaCl_2$	$Mg(OH)_2$	0.5	80–85	Ota et al., 1991
Needle like	~ 20	$Ca(OH)_2$	Na-aluminate	0.05	>50	Ota et al, 1991
Needle like	20–80	$Ca(OH)_2$	$MgCl_2$	0.05	80	Ota et al., 1995
Needle like	?	CaO	MEA, HNO_3	0.33–1	60, 80	Vučak et al., 1997
Needle like	?	Scallop shell	$SrCO_3$	0.13	35	Sasaki et al., 1998a
Needle like	~ 10	Scallop shell	$MgCl_2$	0.03–0.06	35	Sasaki et al., 1998b
Needle like, Columnar	10–20	$Ca(OH)_2$	NaOH, KOH	2–10 L/min/kg CaO	20–80	Konno et al., 2000
Needle like	4–15	$Ca(OH)_2$	H_3PO_4	0.21–0.83	?	Wang et al., 2004
Needle like	~ 10	$Ca(OH)_2$	$MgCl_2$	0.1	80	Ahn et al., 2004
Branched	–	$Ca(OH)_2$	$MgCl_2$	0.1	80	Ahn et al., 2004
Needle like	3–10	$Ca(OH)_2$	$MgCl_2$, Phthalic acid	0.025	80	Park et al., 2008
Needle like	8–16	$Ca(OH)_2$	$MgCl_2$	0.98–1.75	70	Hu et al., 2009
Needle like	4–6	$Ca(OH)_2$	$MgCl_2$, $SrCO_3$	0.1	30	Kim et al., 2009
?	?	$Ca(NO_3)_2$	NH_3, N_2, NH_4OH, HNO_3	?	25	Matsumoto et al., 2010
Needle like	?	$Ca(OH)_2$	$MgCl_2$, Sonication	0.24–0.36	>30	Santos et al., 2012
Needle like	10–12	$CaCl_2$	NH_3	1.0	80	Ding et al., 2018
Branched	–	$CaCl_2$	NH_3	1.0	80	Ding et al., 2018
Needle like	?	$CaCl_2$	MgO, $MgCl_2$, Amine, NaOH	0.08–5.0	>30	Rivera and Van Gerven, 2020
Needle like	?	$Ca(OH)_2$	NaOH	?	40–80	Sakaguchi et al., 2021
Needle like	2–10	$Ca(OH)_2$	NaOH	?	40–80	Sakaguchi et al., 2022
Needle like	?	$CaCl_2$	MEA	3.0	70	Mao et al., 2023

Lime and slaked lime as the Ca source

The carbonation of lime is an industrial method. The lime becomes slaked lime [$Ca(OH)_2$] in water. Calcium carbonate was produced by injecting gaseous CO_2 into a $Ca(OH)_2$ suspension in water as follows:

$$Ca^{2+}\ (aq) + 2OH^-\ (aq) + CO_2\ (aq) \rightarrow CaCO_3\ (s) + H_2O\ (l) \quad (1).$$

This method can provide pure calcium carbonate precipitates. However, most of the precipitated crystals are calcite. Moreover, it is difficult to modify the conditions for synthesizing aragonite because of the relatively low solubility of $Ca(OH)_2$ in water (Ding et al., 2018), as listed in Table 2 (Kendall, 1912; Linke and Seidell, 1958; Duchesne and Reardon, 1995). Two methods have succeeded in precipitating aragonite without additives or external stimuli (Fig. 4).

Method 1: Columnar aragonite is synthesized by precisely controlling the temperature and CO_2 gas feed rate (Fig. 4a: Reactor 1) (Murakami et al., 1977). First, the temperature was maintained at a controlled range of 5–20 °C, and the CO_2 feed rate was set at 7–15 mL/min for 1 g $Ca(OH)_2$ until the carbonation rate reached 2–10%. Subsequently, the CO_2 feed rate was regulated between 0.5 and 2 mL/min for 1 g $Ca(OH)_2$ at temperatures between 7–25 °C until the carbonation rate reached 10–60 %. Thirdly, the temperature was maintained at a level exceeding 45 °C, while the CO_2 feed rate was regulated at a rate exceeding 2 mL/min for a quantity of 1 g $Ca(OH)_2$. The authors do not provide a clear rationale for the success of this three steps method, however, it may control the pH by changing the feed rate of CO_2 gas. In the initial stage of the process, the elevated pH was rapidly reduced by introducing the gas with a relatively high feeding rate. This may result in an optimal pH for aragonite formation. In the second step, the feeding rate was reduced, and the

Table 2. Solubility of Ca-bearing minerals in water

Ca-bearing Minerals	Solubility in water at 25 °C (mol/kg)	Reference
$Ca(OH)_2$	0.0222	Duchesne and Reardon, 1995
$CaCl_2 \cdot 6H_2O$ (Antarcticite)	7.5	Linke and Seidell, 1958
$Ca(NO_3)_2$	8.4	Linke and Seidell, 1958
$CaCO_3$ (Calcite)	1.4×10^{-4}	Kendall, 1912
$CaCO_3$ (Aragonite)	1.5×10^{-4}	Kendall, 1912

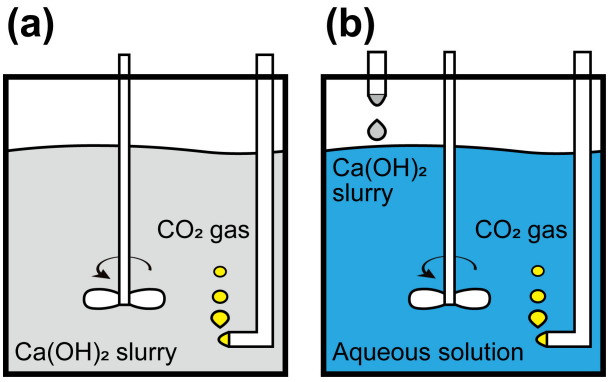

Figure 4. Conventional carbonation methods to synthesize aragonite using $Ca(OH)_2$ as a Ca source at an elevated temperature. (a) Reactor 1: Control of CO_2 gas feed rate for $Ca(OH)_2$ saturated slurry. (b) Reactor 2: Control of Ca concentration and CO_2 gas feed rate.

pH was maintained at a relatively constant level. In the third step, an elevated temperature may be preferable for aragonite formation.

Method 2: aragonite, in the form of needle-like crystals, including a small amount of calcite, was synthesized by gradually adding a $Ca(OH)_2$ aqueous slurry (at a rate of less than 150 mL/min) to 1 L of hot water (at a temperature exceeding 70 °C) while introducing carbon dioxide (Fig. 4b: Reactor 2) (Ota et al., 1986). Although the reason for the success of this method remains unclear, the pH of the starting solution was maintained at a low level due to the absence of a $Ca(OH)_2$ slurry. The addition of a $Ca(OH)_2$ slurry may result in an increase in pH, but the degree of the change in pH can be controlled by introducing CO_2 gas to the solution. Consequently, the synthesis of aragonite seems to be dependent on the pH and temperature.

These two methods reduce the degree of supersaturation of $CaCO_3$. However, additives and external stimuli are commonly used for the rapid, efficient, and convenient synthesis of aragonite crystals.

Additives, temperature, pH, and external stimuli. Various additives such as sucrose (Bennett and Gardiner, 1967; Ota et al., 1986), monoethanolamine (MEA) and HNO_3 (Langelin et al., 1984; Vučak et al., 1997), $MgCl_2$ (Ota et al., 1995; Ahn et al., 2004; Park et al., 2008; Hu et al., 2009), H_3PO_4 (Wang et al., 2004), and sodium aluminate (Ota et al., 1991) in Reactor 1 (Fig. 4a) and NaOH or KOH (Konno et al., 2000; Sakaguchi et al., 2021; Sakaguchi et al., 2022) in Reactor 2 (Fig. 4b) were confirmed to be effective in the synthesis of aragonite.

Aragonite was precipitated when $Ca(OH)_2$ dissolved in a sucrose solution reacted with CO_2 gas at high temperature (Bennett and Gardiner, 1967). The preferred synthetic conditions for aragonite were 20–50 wt% sucrose, 0.05–0.5 M $Ca(OH)_2$, a pH between 7 and 9, and temperatures ranging from 60 to 90 °C. The sucrose should be pure in the absence of organic acids; otherwise, calcite will be obtained.

Monoethanolamine (MEA)–HNO_3 solution has been used to remove impurities from CaO by selective hydroxide precipitations such as $Mg(OH)_2$, $Fe(OH)_3$, and $Al(OH)_3$ (Langelin et al., 1983). This is because the source rock of calcium in their study was dolomite, which contains Mg ions as impurities. The reaction is shown below:

$$CaO\ (s) + 2H^+\ (aq) + CH_2OH^-CH_2NH_2\ (l) \rightarrow Ca^{2+}\ (aq) + CH_2OH^-CH_2NH_3^+\ (aq) + OH^-\ (aq) \quad (2),$$

$$Ca^{2+}\ (aq) + 2OH^-\ (aq) + CO_2\ (aq) \rightarrow CaCO_3\ (s) + H_2O\ (l) \quad (1').$$

In this experiment, needle-like aragonite has been synthesized by precisely controlling the temperature and CO_2 feed rate (Langelin et al., 1984; Vučak et al., 1997). In addition to removing the impurities using MEA, various aliphatic amines, diamines, and amino acids as additives influence the polymorphs and morphology of calcium carbonates (Chuajiw et al., 2014). Both hydrophilic functional groups and hydrophobic alkyl groups appear to influence the polymorphs and morphology of the precipitated $CaCO_3$ particles.

The addition of $MgCl_2$ to water succeeded in synthesizing needle-like aragonites with aspect ratios ranging from 8 to 80 (Ota et al., 1995; Sasaki et al., 1998b; Ahn et al., 2004; Park et al., 2008; Kim et al., 2009; Hu et al., 2009; Santos et al., 2012). In numerous experiments, the temperature was maintained at 70–80 °C. However, in cases where specific seed crystals, additional additives, or external stimuli were present, aragonite could be synthesized at relatively low temperatures, above 30 °C (Table 1). The presence of Mg^{2+} in water enhances the precipitation of aragonite rather than calcite.

Aragonite was synthesized by mixing a CO_2-dissolved NaOH solution and $Ca(OH)_2$ slurry (Konno et al., 2000; Sakaguchi et al., 2021; Sakaguchi et al., 2022). The addition of CO_2 gas into the alkali solutions increased the dissolved Na_2CO_3 or K_2CO_3 species in water. Calcium carbonate was precipitated via the reaction between $Ca(OH)_2$ and $NaCO_3$ or K_2CO_3 in water:

Preparation of a CO_2-dissolved solution:

$$2OH^-(aq) + CO_2(aq) \rightarrow CO_3^{2-}(aq) + H_2O(l) \quad (3).$$

Mixing Ca- and CO_2-dissolved solutions:

$$Ca^{2+}(aq) + CO_3^{2-}(aq) \rightarrow CaCO_3 \quad (4).$$

Needle-like aragonite was precipitated at higher temperatures (40–80 °C). The diameter of the needle-like aragonite particles increased with the increase in temperature.

A high-gravity environment also precipitated needle-like aragonite with H_3PO_4 as an additive (Wang et al., 2004). The addition of H_3PO_4 is essential for synthesizing aragonite. A high-gravity environment influences the size distribution of the synthesized particles and reaction times. This is likely to be owing to the enhancement of the mixing state of the reagents (Chen et al., 2000). The high gravity is of an order several hundred or thousand times larger than that of the gravity on the Earth's surface. The aragonite content relative to calcite and the aspect ratio of the needle-like aragonite were altered by the rotating speed of the reactor (Wang et al., 2004). At lower rotating speeds, the micro-mixing was not optimal. Furthermore, an inhomogeneous supersaturation ratio existed depending on the local area, resulting in increased calcite growth. At higher rotating speeds, the micro-mixing intensified, leading to a higher supersaturation ratio and calcite precipitation.

External stimuli of sound wave (Zhou et al., 2004; Santos et al., 2012) have been tested to synthesize aragonite. Sound waves in the range of 16–100 kHz induce the formation of small cavities or microbubbles in solution. The sonication system requires a cooling bath to lower the temperature generated by sound waves. The collapsing microbubbles produce high local temperatures, pressures, and shear forces. This method has successfully produced aragonite (Santos et al., 2012). The polymorph ratios, size, and morphology of crystals were altered by several process parameters, namely, the Mg/Ca ratio, ultrasound amplitude, continuous ultrasound, sonication time applied to the $Ca(OH)_2$ slurry before introduction of CO_2 gas (ultrasound pre-breakage), CO_2 feed rate, and concentration of $Ca(OH)_2$.

$CaCl_2$ and $Ca(NO_3)_2$ as the Ca source

As an alternative source of Ca ion, calcium chloride ($CaCl_2$) and calcium nitrate [$Ca(NO_3)_2$] have been tested (Ota et al., 1991; Matsumoto et al., 2010; Ding et al., 2018; Rivera and Van Gerven, 2020; Mao et al., 2023).

Additives, temperature, pH, and external stimuli. In this case, additives such as NH_3, NaOH, and KOH are required to provide OH^- in water. Calcium carbonate is produced by injecting CO_2 gas into a $CaCl_2$-NH_3 aqueous solution (Ding et al., 2018) as follows:

$$NH_3\ (aq) + H_2O\ (l) \rightarrow NH_4^+\ (aq) + OH^-\ (aq) \quad (5),$$

$$Ca^{2+}\ (aq) + 2OH^-\ (aq) + CO_2\ (aq) \rightarrow CaCO_3\ (s) + H_2O\ (l) \quad (1').$$

The difference with $Ca(OH)_2$ as the Ca source is the concentration of Ca^{2+} and OH^- ions. Needle-like aragonite has been synthesized in a $CaCl_2$-NH_3-CO_2 aqueous system at 80 °C (Ding et al., 2018). Plate-shaped vaterite was formed at the beginning of the reaction (10 min). A phase transformation from vaterite to aragonite was observed at a reaction time of 30 min. Most of the vaterite transformed into needle-like aragonite at 60 min. The formation of vaterite at the beginning of the reaction was interpreted using Ostwald's rule (wherein the least stable polymorph crystallizes first rather than stable ones). The phase transformation from vaterite to aragonite, rather than calcite, was interpreted as the kinetics at high temperatures.

As an external stimuli, $CO_2/NH_3/N_2$ microbubbles were supplied continuously to an aqueous $Ca(NO_3)_2$ solution, and aragonite was synthesized under constant pH (9.7–10.5) conditions at 298 K (Matsumoto et al., 2010). The solution pH was maintained constant by adding HNO_3 and NH_4OH solutions. The average bubble size was maintained at 40–1000 μm by controlling the rotation rate of the bubble generator and N_2 flow rate. The polymorphs of vaterite and calcite were predominantly synthesized at pH of 9.0 and 11.0, respectively.

Table 3. Aragonite crystal growth from aragonite seed crystals

Morphology	Aspect ratio	Ca source	Seed crystal	CO_2 feed rate (CO_2 gas, L/min/Solution, L)	T (°C)	Reference
Needle like	20–35	$Ca(OH)_2$	Aragonite	?	50–80	Tanaka et al., 1988
Needle like	~ 20	$Ca(OH)_2$	H_3PO_4	0.0027–0.033	30–80	Shibata et al., 1991

ARAGONITE GROWTH ON SEED CRYSTALS

The crystal growth from the aragonite seed crystals was tested to control the particle size and morphology, as listed in Table 3. Needle-like aragonite was obtained by adding the columnar seed crystals of aragonite to a $Ca(OH)_2$-CO_2 aqueous system at >50 °C (Tanaka et al., 1988). The elongated aragonite crystals were obtained at the pH range from eight to nine. The pH was controlled by the concentration of columnar aragonite seed crystals. This implies that, in addition to the effect of pH, the quantity of seed crystals may also affect the polymorphs and morphology of the precipitate. Needle-like long aragonite has also been obtained by the addition of aragonite seed crystals and H_3PO_4 salts (Shibata et al., 1991). This method can inhibit the coagulation of aragonite particles. Therefore, the presence of H_3PO_4 may prevent aragonite particle aggregation.

PURE ARAGONITE SYNTHESIS

The synthesis of pure aragonite is a desirable objective, as it serves as a reinforcing material that can help to avoid the introduction of unwanted complications resulting from the presence of impurities. In this review, the criterion for pure aragonite was defined as a composition of >90 % aragonite in the polymorphs, as determined by the XRD analysis. Pure aragonite was synthesized by various carbonation methods (Ota et al., 1995; Sasaki et al., 1998b; Konno et al., 2000; Wang et al., 2004; Park et al, 2008; Hu et al., 2009; Kim et al., 2009; Matsumoto et al., 2010; Santos et al., 2012; Rivera and van Gerven, 2020; Sakaguchi et al., 2022; Mao et al., 2023). Identifying the optimal conditions for pure aragonite formation is a challenging. However, research has indicated that pH levels around 9, low CO_2 feed rates, the addition of amine or Mg ions, and elevated temperatures are conducive to achieving this goal.

CONTROL OF ASPECT RATIO

The aspect ratio of aragonite influences the elastic modulus of a composite material as predicted by the Halpin-Tsai model (Fig. 2). The preferred aspect ratio for reinforcement materials is between 50 and 100 as expected by the Halpin-Tsai model, though, the aspect ratio of synthetic aragonite is typically around 10, as listed in Tables 1 and 3. An aspect ratio greater than 20 was achieved through crystal growth in the presence of aragonite seed crystals or $MgCl_2$ as an additive. However, the factors controlling the aspect ratio are not yet fully understood.

The aspect ratio of aragonite particles varies marginally depending on the concentration of the H_3PO_4 additive under high-gravity conditions (Wang et al., 2004). In this experiment, 7.0 g/L of H_3PO_4 was the best condition to obtain a high aspect ratio of 10–15 as shown in Figure 5. A potential role of H_3PO_4 was the generation of needle-like hydroxylapatite (HAP) as a reaction between H_3PO_4 and the $Ca(OH)_2$ slurry. HAP functioned as a heterogeneous nucleator, and needle-like aragonite grew on it. When the H_3PO_4 concentration was excessively high, aragonite aggregated and formed irregular shapes.

The Mg/Ca ratio influences the aspect ratio of aragonite (Park et al., 2008), as shown in Figure 6. As the Mg^{2+} ion concentration increased, the aspect ratio increased until a concentration of 71 mol%. This is likely to have been owing to the transition of polymorphs from Mg-calcite to aragonite. The aspect ratio decreased with the increase in Mg/Ca ratios above 75 mol%. The role of the Mg ions was interpreted as the promotion of growth along the major axis of the needle-like crystals through a selective side poisoning mechanism. When the Mg/Ca ratio was higher than 75 mol%, Mg^{2+} was adsorbed on various crystal faces, and the relative growth of the minor axis increased. This resulted in a decrease in the aspect ratio.

The highest aspect ratio of aragonite was obtained in the presence of $MgCl_2$ as an additive (Ota et al., 1995) as shown in Figure 3a. The Mg/Ca ratio was 0.76 mol $MgCl_2$/0.5 mol $Ca(OH)_2$ = 1.52 (= 60 mol%). This Mg concentration is similar to the optimal concentrations (71–75 mol%) reported in a similar work (Park et al., 2008), although the aspect ratio is different. The difference in the CO_2 gas feed rate of 0.05 and 0.025 (L_{CO2}/min/$L_{solution}$) may have influenced the aspect ratio. Here, L_{CO2} and $L_{solution}$ are the volumes (Litre) of CO_2 gas and aqueous solution, respectively.

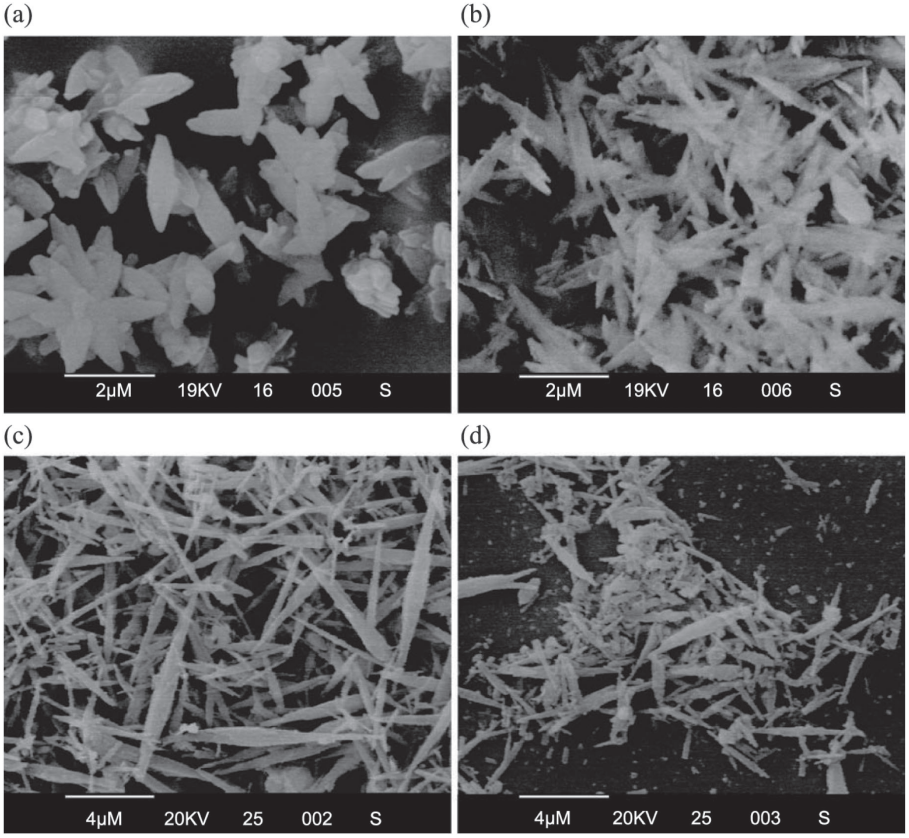

Figure 5. Morphology of synthesized $CaCO_3$ particles as a function of H_3PO_4 concentrations (a) 0 g/L, (b) 3.5 g/L, (c) 7.0 g/L, and (d) 10.5 g/L. The main polymorphs of $CaCO_3$ particles are (a) calcite and (b)–(d) aragonite (Wang et al., 2004). Reprinted with permission from Elsevier.

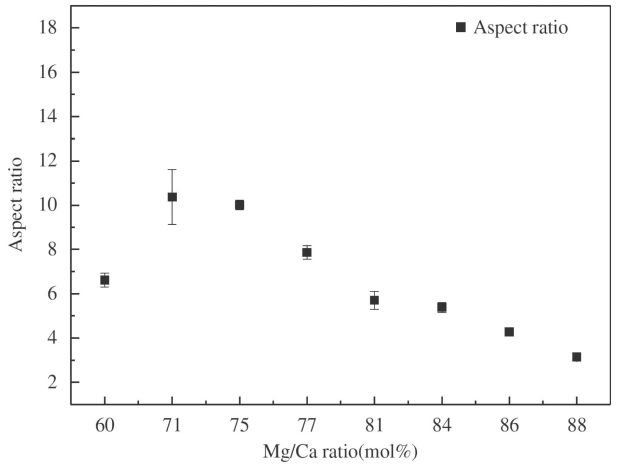

Figure 6. Aspect ratio of aragonite as a function of Mg/Ca ratio (Park et al., 2008). Reprinted with permission from Elsevier.

DISCUSSIONS: KEY FACTORS OF THE ARAGONITE FORMATION

The critical factors include the additives, Ca source, CO_2 feed rate, pH, and temperature. Herein, these factors are discussed to understand the mechanism of aragonite synthesis.

Additives

Influence of Mg ions. The mechanism of aragonite precipitation in the presence of Mg^{2+} ions has been interpreted as the inhibition of calcite crystal growth by the adsorption of hydrated Mg ions on the calcite surface (De Groot and Duyvis, 1966; Reddy and Nancollas, 1976). An atomic-force-microscopy study (Davis et al., 2000) reported that the enhanced mineral solubility of Mg-incorporated calcite reduces calcite growth. However, this mechanism may not be simple (Ahn et al., 2004; Ramakrishna et al., 2017; Boon et al., 2020). Density functional theory calculations indicate that the presence of Mg ion on a calcite surface alters the surface energy and influences the subsequent adsorption of ions and water molecules (Sakuma et al., 2014; Andersson et al., 2016). The nucleation of aragonite was predicted by the DFT study to occur at higher Mg/Ca ratios (>2) in solution, indicating that the alteration of the surface energy by the dissolved Mg and Ca ions inhibits the calcite nucleation rather than the increased solubility mechanism (Sun et al., 2015). The addition of $MgCl_2$ decreases the pH by the precipitation of $Mg(OH)_2$ at elevated pH (Hu et al., 2009). This results in an increase in the Ca^{2+} ions dissolved from $Ca(OH)_2$. The increased solubility of $Ca(OH)_2$ may be related to the formation of aragonite.

Table 4. Lattice parameters of calcite, aragonite, and seed crystals of strontianite ($SrCO_3$), and hydroxylapatite (HAP)

Crystals	Crystal systems	*a* (Å)	*b* (Å)	*c* (Å)	Reference
Calcite	Trigonal system using hexagonal axes	4.990	4.990	17.062	Graf, 1961
Aragonite	Orthorhombic	4.961	7.967	5.740	De Villiers, 1971
Strontianite ($SrCO_3$)	Orthorhombic	5.090 (+2.6%)*	8.358 (+4.9%)*	5.997 (+4.5%)*	De Villiers, 1971
Hydroxylapatite (HAP)	Hexagonal	9.417	9.417	6.875	Hughes et al., 1989

*The percentage indicates the difference from those of aragonite.

Enhancement of aragonite nucleation. The presence of seed crystals such as aragonite and $SrCO_3$ enhances the precipitation of aragonite (Tanaka et al., 1988; Shibata et al., 1991; Sasaki et al., 1998a; Kim et al., 2009). $SrCO_3$ was selected because the difference in the lattice parameters is less than 5% of those of aragonite (as listed in Table 4) and $SrCO_3$ crystals are more stable in water than metastable aragonite (Sasaki et al., 1998a). A potential role of H_3PO_4 is the formation of needle-like HAP before the precipitation of calcium carbonate. Aragonite may have nucleated on the needle-like HAP after the start of carbonation. Because the lattice parameters of HAP are not similar to those of aragonite, as listed in Table 4, the surface structure may be related to the nucleation of aragonite. The aragonite formation on the seed crystal implied that the barrier to aragonite formation was reduced by the presence of seed crystals.

What is the role of elevated temperature?

Most aragonite was synthesized at higher temperatures (>50 °C). The effect of higher temperatures can be understood from attempts at aragonite synthesis at lower temperatures. The reaction temperature can be lowered by including seed crystals of aragonite and $SrCO_3$ in the solution (Shibata et al., 1991; Sasaki et al., 1998a; Kim et al., 2009). It can thus be concluded that elevated temperatures may be a prerequisite for the nucleation of aragonite in the absence of seed crystals, external stimuli, and $MgCl_2$. The sonication technique with the $MgCl_2$ additive successfully synthesized aragonite at low temperatures (<30 °C) (Santos et al., 2012). The mechanism was explained by the localized high-temperature field in the solution created by sonication, which resulted in the nucleation of aragonite seeds. Aragonite was synthesized at 25 °C using the CO_2/NH_3 microbubble technique (Matsumoto et al., 2010). The reason for the successful synthesis of aragonite at low temperature is not clear, but the microbubble may alter the nucleation stage of aragonite by the local pH near the gas-liquid interface, which can differ from the overall pH in the bulk liquid. This difference may alter the supersaturation at the gas-liquid interface and thereby, result in the selective synthesis of aragonite, calcite, and vaterite depending on the pH of the bulk liquid. These observations imply that the temperature influences the nucleation stage of aragonite.

Role of the solution pH

The chemical species of CO_2 dissolved in water vary with pH. At pH < 6, H_2CO_3 is the major species, whereas HCO_3^- and CO_3^{2-} are dominant at pH > 6. This was calculated using the PhreeqC program (Parkhurst and Appelo, 2013) (Fig. 7). To precipitate calcium carbonate, the presence of ionic species HCO_3^- and CO_3^{2-} is preferable. Therefore, a high pH (>6) is preferable for synthesizing calcium carbonates. The pH of the solution was also used to determine the degree of $CaCO_3$ precipitation when $Ca(OH)_2$ was used as the Ca source. Before feeding the CO_2 gas, the pH of the solution was high (~ 12) due to the dissolution of $Ca(OH)_2$. The hydroxide ion concentration

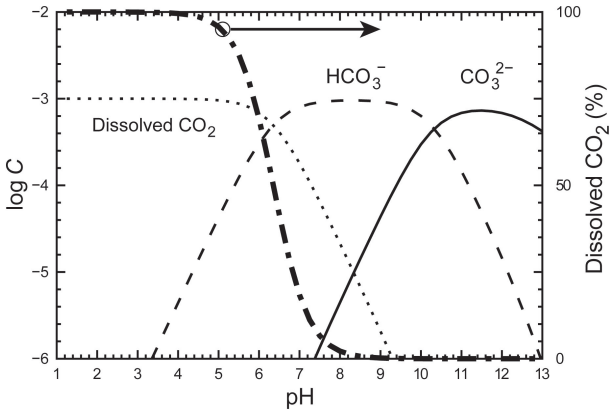

Figure 7. Chemical species of CO_2 (1 mmol/kg) dissolved in water at 25 °C (CO_3^{2-}: solid line; HCO_3^-: dashed line; and dissolved CO_2: dotted line), along with the percentage of dissolved CO_2 [CO_2(aq) and H_2CO_3] (long dashed short dashed line) as simulated by the PhreeqC program using the minteq.v4 database. Here *C* represents the concentration of chemical species (mol/kg). An arrow indicates that the vertical axis of the percentage of dissolved CO_2 is on the right.

decreased upon feeding of CO_2 gas as shown in Reaction 1. When all the $Ca(OH)_2$ had reacted with CO_2 gas, the pH became constant at ~ 8.

The polymorph is dependent on the pH. The production yield of vaterite synthesized in pH-controlled experiments conducted at 30 °C demonstrated a positive correlation with decreasing pH, reaching a maximum at pH < 8.2 (Chen et al., 1997). The maximum yield of calcite was observed at a pH of 8.6. In their experiments, the temperature was maintained at a relatively low level, and no additive were employed to facilitate aragonite synthesis. However, the presence of a small amount of aragonite was confirmed at pH values exceeding 8.6. The synthesis employing the microbubble technique unambiguously revealed that the maximum production rates of vaterite, aragonite, and calcite were at pH 9, 9.5, and 11, respectively (Matsumoto et al., 2010). At higher pH values, the concentration of chemical species of CO_3^{2-} increases (Fig. 7), resulting in the attainment of supersaturation conditions that are higher than usual. Such conditions may result in a change in the calcium carbonate polymorph. Calcite exhibits a preference for high supersaturation conditions, whereas aragonite and vaterite display a preference for low supersaturation conditions.

The pH of the solution is critical for the selective precipitation of impurities as metal hydroxides. The chemical species of Ca, Fe, Al, and Mg in water were estimated as functions of pH using the PhreeqC program (Fig. 8). Ca is dissolved as Ca^{2+} at a low pH and as $Ca(OH)^+$ at exceptionally high pH. It does not precipitate as $Ca(OH)_2$. Fe precipitates as $Fe(OH)_3$ at pH > 2. Al precipitates as $Al(OH)_3$ at a low pH (>4), although it redissolves as $Al(OH)_4^-$ at pH > 6. Fe and Al can be conveniently removed as hydroxides by lowering the pH of the solution.

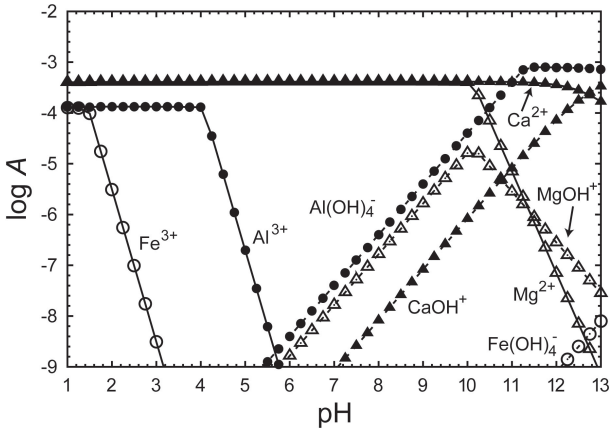

Figure 8. Chemical species of metals in water as a function of solution pH at 25 °C simulated by PhreeqC program using the minteq.v4 database. Here, *A* is the activity of each species (mol/kg).

Mg is dissolved as Mg^{2+} and $MgOH^+$ species at pH < 10. However, it precipitates as $Mg(OH)_2$ at higher pH. This is consistent with certain experiments using Mg^{2+} ions as an additive, where the precipitation of brucite [$Mg(OH)_2$] at pH > 10 and dissolution of $Mg(OH)_2$ at lower pH were verified (Ahn et al., 2004).

Supersaturation of $CaCO_3$: Ca^{2+} and CO_2 concentrations

Both nucleation and crystal growth depend on the supersaturation of the solution. The solubility products of calcite and aragonite at 25 °C are 3.3×10^{-9} and 5.0×10^{-9}, respectively (U.S. Environmental Protection Agency, 1998). The calcium concentration in the majority of carbonation methods is adequate for the precipitation of calcium carbonates, indicating that the feeding rate of CO_2 gas exerts control over the degree of supersaturation. Needle-like aragonite was synthesized under low-supersaturation conditions, whereas calcite was precipitated under high-supersaturation conditions (Hu and Deng, 2003).

In the process of using the MEA and HNO_3 solution, a high concentration of CO_2 gas in air (>99.6%) shortened the carbonation reaction time compared with the gas mixture (33% CO_2) (Vučak et al., 1997). Meanwhile, the ratio of needle-like aragonite to calcite increased with 33% CO_2 compared with pure CO_2. This is consistent with the observations wherein the transformation from aragonite to calcite was reduced at a lower feed rate of CO_2 gas (0.008 $L_{CO2}/min/L_{solution}$) from that at 0.04 $L_{CO2}/min/L_{solution}$ (Langelin et al., 1984). The content of aragonite also increased with the decrease in the CO_2 feed rate when synthesized under ultrasound with $MgCl_2$ as the additive (Santos et al., 2012) and in a high-gravity environment with H_3PO_4 as the additive (Wang et al., 2004). These explained the aragonite formation owing to the low supersaturation due to relatively low concentration of CO_3^{2-} in the reaction zone. It should be noted that in their experiments as well, H_3PO_4 enhanced the formation of aragonite by providing a seed crystal formed in water.

In the majority of carbonation processes, the concentration of CO_3^{2-} is significantly lower than that of Ca^{2+}. Consequently, the degree of supersaturation of $CaCO_3$ can be regulated by controlling the concentration of CO_3^{2-}. The concentration of CO_3^{2-} ions is significantly affected by the solution pH, as shown in Figure 7, and maintaining pH control is critical with regard to the polymorphism. In the case of a liquid-liquid synthesis, such as the mixing of $CaCl_2$ and Na_2CO_3 solutions, a high concentration of CO_3^{2-} ions can be achieved, allowing for concentration of Ca^{2+} ions to be used to control the supersaturation degree. In this case, aragonite can be formed even at

high pH conditions when the concentration of Ca^{2+} is sufficient for realizing a moderate supersaturation degree. Needle-like aragonite was synthesized by gradually adding a $Ca(OH)_2$ aqueous slurry to water while introducing carbon dioxide (Fig. 4b) (Ota et al., 1986). This method realized low-supersaturation conditions by reducing the concentration of Ca ions in water.

External stimuli

Two effects of sonication on the aragonite formation were considered. One is the local high temperature around the imploding cavities, and the other is the generation of nucleation sites. The addition of $MgCl_2$ was required to synthesize aragonite in the carbonation method (Santos et al., 2012). The reason for the requirement of $MgCl_2$ is not clear. However, it may be related to the supersaturation of $CaCO_3$ in the solution.

Small microbubbles have certain advantages for crystal synthesis. These include an increase in the gas-liquid interface, which increases the reaction field and the average residence time of the bubbles by decreasing the buoyancy (Matsumoto et al., 2010). The local pH at the gas-liquid interface depends on the mixture ratio of CO_2 and NH_3 gas. CO_2 gas decreases the local pH, whereas NH_3 gas increases it. When the local pH is higher than the solution pH, the degree of supersaturation of $CaCO_3$ at the interface should increase. Therefore, calcite precipitation is preferable. Meanwhile, a low local pH decreases the supersaturation of $CaCO_3$ at the interface. This results in vaterite precipitation. The optimal pH value for aragonite is between the local pH values.

DISCUSSION ON THE ARAGONITE MORPHOLOGY

Crystal faces of aragonite

Aragonite is an orthorhombic carbonate with space group *Pmcn* (Speer, 1983). Its lattice parameters under ambient conditions are listed in Table 4. The experimentally observed morphology of single-crystal aragonite is shown in Figure 9. Three habits are commonly reported (Klein and Dutrow, 2007): (1) Needle-shaped (acicular pyramidal)—planes (Fig. 9a) consisting of long {010} and {110} planes terminated by a significantly steep dipyramid and {011}. (2) Tabular (Fig. 9b)—consisting of a prominent {010} modified by {110} and a low prism {011}. (3) Pseudohexagonal twins (not shown in Fig. 9)—consisting of three individuals twinned on {110} terminated by a basal plane.

The surface energy of crystal faces may determine the morphology of crystals. These have been evaluated

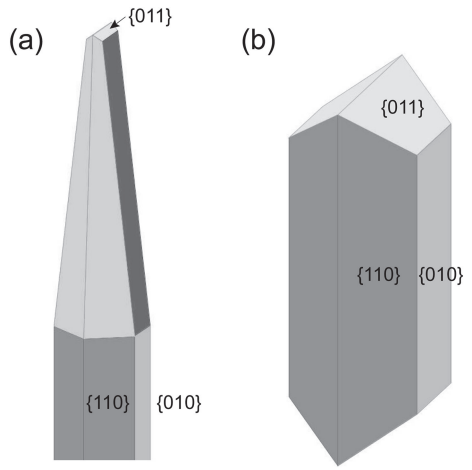

Figure 9. Morphology and crystal faces of common aragonite. Numbers indicate the Miller indices of the set of all symmetrically equivalent crystal faces. A tip of (a) needle shape and (b) tabular shape. The crystal shapes were created by JCrystal (Weber, 2011).

by atomistic simulations (De Leeuw and Parker, 1998; Akiyama et al., 2011; Sekkal and Zaoui, 2013; Massaro et al., 2014; Kawano et al., 2015). The surface energy of the low-Miller-index surfaces revealed that the commonly observed {011} faces were the most stable face among the calculated low-index surfaces (De Leeuw and Parker, 1998; Massaro et al., 2014) in dry and wet conditions. However, the other commonly observed {110} and {010} faces were comparable to the other tested faces (De Leeuw and Parker, 1998; Akiyama et al., 2011; Massaro et al., 2014). The estimated equilibrium morphology of aragonite based on these surface energies and the Wulff and Gibbs theorem (Wulff, 1901; Gibbs, 1928) was inconsistent with the experimentally observed morphology. The discrepancy between the experimental and modeled morphologies has not been adequately elucidated. One hypothesis is that the surface energy in the classical model can be modified by the presence of adsorbed ions, such as magnesium ions. This phenomenon was not considered in the papers. Meanwhile, the estimated growth morphology was similar to the experimentally observed tabular morphology (De Leeuw and Parker, 1998).

The anisotropic crystal habits of aragonite such as its needle-like morphology, cannot be explained only by the equilibrium and growth morphology. This also requires the variation in the growth rate of the crystal faces. The growth rate may vary as a function of temperature, degree of supersaturation, and selective adsorption of water and additives. For example, the presence of a local dipole moment on a particular surface of an ionic crystal enhances the adsorption of polar impurities including water molecules. At high supersaturation, the removal of adsorbed

molecules may become the rate-determining step for the growth of the face (Hartman, 1973). From density-functional-theory calculations, the adsorption energy of Mg ion is different between the {001} and {110} faces of aragonite (Kawano et al., 2015). This difference in the adsorption energy of ions can alter the crystal habit of aragonite.

The anisotropic crystal habits of aragonite such as its needle-like morphology, cannot be explained only by the equilibrium and theoretically estimated growth morphology. This also requires the variation in the growth rate of the crystal faces. The growth rate may vary as a function of temperature, degree of supersaturation, and selective adsorption of water and additives. For example, the presence of a local dipole moment on a particular surface of an ionic crystal enhances the adsorption of polar impurities including water molecules. At high supersaturation, the removal of adsorbed molecules may become the rate-determining step for the growth of the face (Hartman, 1973). From density-functional-theory calculations, the adsorption energy of Mg ion is different between the {001} and {110} faces of aragonite (Kawano et al., 2015). This difference in the adsorption energy of ions can alter the crystal habit of aragonite.

Elastic modulus of calcite and aragonite along certain crystal directions

The Halpin-Tsai model implies that the strength of the composite depends on the elastic modulus and aspect ratio of aragonite. The Young's modulus depending on the crystal axis can be calculated from the elastic compliance constant of crystals (Nye, 1957). The elastic compliance constants of various crystals were summarized in a paper (Huntington, 1958) and those of aragonite (Voigt, 1907) and calcite (Voigt, 1890; Bhimasenacrar, 1945) were used for estimating the Young's modulus. The calculated Young's moduli along the typical crystal axes are listed in Table 5.

The calcite surface is characterized by the {104} cleavage. The Young's modulus parallel to the [104] direction normal to the cleavage plane is 58.6 GPa. The long axis of needle-like aragonite is parallel to the [001] direction. The Young's modulus 82.0 GPa is higher than that of the calcite perpendicular to the cleavage. Therefore, the difference in the tensile strength of the composite originating from the difference in the polymorphs of calcite and aragonite is owing to the differences in the aspect ratio and Young's modulus based on the Halpin-Tsai model. If the long axis of aragonite is parallel to the [100] direction, the Young's modulus can be 1.7 times higher than that of the commonly observed needle-like aragonite elongated parallel to the [001] direction. Such controlled crystal growth should be studied further for the development of novel aragonite fillers.

CONCLUDING REMARKS

Two methods are commonly used for calcium carbonate synthesis with gaseous CO_2. The first is the injecting gaseous CO_2 into a $Ca(OH)_2$ slurry. The second is adding a $Ca(OH)_2$ slurry to CO_2 gas-injected water. Both methods control the concentrations of CO_2 and Ca ions in the solutions. In both methods, low supersaturation of $CaCO_3$ is preferable for synthesizing aragonite. Additives such as $MgCl_2$, ammonia, amines, nitric acid, sucrose, H_3PO_4, NaOH, and KOH are critical for synthesizing aragonite. The mechanism of aragonite precipitation is not fully understood. However, most additives alter the pH and supersaturation of $CaCO_3$, and certain additives function as aragonite seed crystals. The pH of the solution should be higher than eight. This is related to the chemical species of the dissolved CO_2 gas in the water. The chemical species HCO_3^- and CO_3^{2-} are common at higher pH. When Mg ions are included in the solution as additives, the final pH should be lower than 10 to prevent the precipitation of brucite. A high temperature (>50 °C) is preferable for aragonite synthesis, but this temperature can be reduced in the presence of seed crystals. Therefore, temperature is related to the nucleation of aragonite. High-gravity external stimuli can narrow the particle size distribution and reduce the reaction time. The sound wave and microbubble methods can alter the local temperature and pH of the solution, successfully synthesizing aragonite. Controlling the aragonite morphology and crystallographic growth direction is critical to the elastic properties of composite materials. The morphology of aragonite appears to vary with the quantity of seed aragonite crystals or seed hy-

Table 5. Calculated Young's moduli of calcite and aragonite along some crystal directions

Tensile direction	Calcite (Trigonal system using hexagonal axes)	Tensile direction	Aragonite (Orthorhombic system)
[100]	90.9 GPa	[100]	143.9 GPa
[104]	58.6 GPa	[010]	75.8 GPa
[001]	57.8 GPa	[001]	82.0 GPa

droxyapatite crystals. The Mg/Ca ratio in water also influences the aspect ratio of the needle-like aragonite. The long axes of most synthetic needle-like aragonites are parallel to the [001] direction. The calculated elastic modulus, depending on the crystallographic direction of aragonite, is anisotropic. If the aragonite elongates parallel to the [100] direction, the Young's modulus along the long axis can be 1.7 times higher than that of the commonly observed aragonite.

ACKNOWLEDGMENTS

We gratefully acknowledge two anonymous reviewers for their constructive reviews.

REFERENCES

Ahn, J.-W., Choi, K.-S., Yoon, S.-H. and Kim, H. (2004) Synthesis of Aragonite by the Carbonation Process. Journal of the American Ceramic Society, 87, 286-288.

Akiyama, T., Nakamura, K. and Ito, T. (2011) Atomic and electronic structures of surfaces. Physical Review B: Condensed Matter and Materials Physics, 84, 085428.

Andersson, M.P., Dideriksen, K., Sakuma, H. and Stipp, S.L.S. (2016) Modeling how incorporation of divalent cations affects calcite wettability-implications for biomineralization and oil recovery. Scientific Reports, 6, 28854.

Bennett, M.C. and Gardiner, S.D. (1967) Improvements in and relating to the manufacture of aragonite. UK Patent, GB-1239407.

Bhimasenacrar, J. (1945) Elastic Constants of Calcite and Sodium Nitrate. Proceedings of the Indian Academy of Sciences. Mathematical Sciences, 22, 199-208.

Boon, M., Rickard, W.D.A., Rohl, A.L. and Jones, F. (2020) Stabilization of Aragonite: Role of Mg^{2+} and Other Impurity Ions. Crystal Growth and Design, 20, 5006-5017.

Chen, P.-C., Tai, C.Y. and Lee, K.C. (1997) Morphology and growth rate of calcium carbonate crystals in a gas-liquid-solid reactive crystallizer. Chemical Engineering Science, 52, 4171-4177.

Chen, J.-F., Wang, Y.-H., Guo, F., Wang, X.-M. and Zheng, C. (2000) Synthesis of nanoparticles with novel technology: High-gravity reactive precipitation. Industrial and Engineering Chemistry Research, 39, 948-954.

Chuajiw, W., Takatori, K., Igarashi, T., Hara, H. and Fukushima, Y. (2014) The influence of aliphatic amines, diamines, and amino acids on the polymorph of calcium carbonate precipitated by the introduction of carbon dioxide gas into calcium hydroxide aqueous suspensions. Journal of Crystal Growth, 386, 119-127.

Davis, K.J., Dove, P.M. and De Yoreo, J.J. (2000) The role of Mg^{2+} as an impurity in calcite growth. Science, 290, 1134-1137.

De Groot, K. and Duyvis, E.M. (1966) Crystal form of precipitated calcium carbonate as influenced by adsorbed magnesium ions. Nature, 212, 183-184.

De Leeuw, N.H. and Parker, S.C. (1998) Surface Structure and Morphology of Calcium Carbonate Polymorphs Calcite, Aragonite, and Vaterite: An Atomistic Approach. The Journal of Physical Chemistry B, 102, 2914-2922.

De Villiers, J.P.R. (1971) Crystal structures of aragonite, strontianite, and witherite. The American Mineralogist, 56, 758-767.

Ding, Y., Liu, Y., Ren, Y., Yan, H., et al. (2018) Controllable synthesis of all the anhydrous $CaCO_3$ polymorphs with various morphologies in $CaCl_2$-NH_3-CO_2 aqueous system. Powder Technology, 333, 410-420.

Duchesne, J. and Reardon, E.J. (1995) Measurement and prediction of portlandite solubility in alkali solutions. Cement and Concrete Research, 25, 1043-1053.

Gibbs, J.W. (1928) The collected works of J. Willard Gibbs, Ph.D, LLD. pp. 434, Longmans, Green and Co., New York.

Graf, D.L. (1961) Crystallographic tables for the rhombohedral carbonates. The American Mineralogist, 46, 1283-1316.

Guan, Z., Lin, Z. and Mai, K. (2013) Monetaria moneta as a novel β-nucleating agent for isotactic polypropylene. Composites Science and Technology, 87, 58-63.

Halpin, J.C. (1969) Effects of environmental factors on composite materials. AFML-TR-67-423, pp. 53, Air Force Materials Laboratory Technical Report.

Halpin, J.C. and Kardos, J.L. (1976) The Halpin-Tsai Equations: A Review. Polymer Engineering and Science, 16, 344-352.

Hartman, P. (1973) Structure and morphology. In Crsytal growth: An introduction (Hartman, P. Ed.). pp. 531, North-Holland Publ. Co., Amsterdam, 367-402.

Ho, H.-J. and Iizuka, A. (2023) Mineral carbonation using seawater for CO_2 sequestration and utilization: A review. Separation and Purification Technology, 307, 122855.

Hu, Z. and Deng, Y. (2003) Supersaturation control in aragonite synthesis using sparingly soluble calcium sulfate as reactants. Journal of Colloid and Interface Science, 266, 359-365.

Hu, Z., Shao, M., Li, H., Cai, Q., et al. (2009) Synthesis of needle-like aragonite crystals in the presence of magnesium chloride and their application in papermaking. Advanced Composite Materials, 18, 315-326.

Hughes, J.M., Cameron, M. and Crowley, K.D. (1989) Structural variations in natural F, OH, and Cl apatites. The American Mineralogist, 74, 870-876.

Huntington, H.B. (1958) The Elastic Constants of Crystals. Journal of Physics C: Solid State Physics, 7, 213-351.

Jimoh, O.A., Ariffin, K.S., Hussin, H.B. and Temitope, A.E. (2018) Synthesis of precipitated calcium carbonate: a review. Carbonates and Evaporites, 33, 331-346.

Jing, Y., Nai, X., Dang, L., Zhu, D., et al. (2018) Reinforcing polypropylene with calcium carbonate of different morphologies and polymorphs. Science and Engineering of Composite Materials, 25, 745-751.

Kawano, J., Sakuma, H. and Nagai, T. (2015) Incorporation of Mg^{2+} in surface Ca^{2+} sites of aragonite: an ab initio study. Progress in Earth and Planetary Science, 2, 7.

Kendall, J. (1912) XCVI. The solubility of calcium carbonate in water. The London, Edinburgh, and Dublin Philosophical Magazine and Journal of Science, 23, 958-976.

Kim, K.-H., Han, G.-C., You, K.-S., Kim, H. and Ahn, J.-H. (2009) Effect of $SrCO_3$ and $MgCl_2$ addition on synthesis of aragonite in $Ca(OH)_2$-CO_2-H_2O system at low temperature. Geosystem Engineering, 12, 21-26.

Klein, C. and Dutrow, B. (2007) The 23rd edition of the manual of mineral science. pp. 675, John Wiley and Sons, Inc, New Jersey.

Konno, H., Doi, R. and Nanri, Y. (2000) The method for manufacturing aragonite cyrstal calcium carbonate. Japan Patent, JP-3902718.

Langelin, H.R., Delannoy, A., Nicole, J. and Hennion, J. (1983) Nouveau procédé de préparation industrielle de carbonates de calcium de synthèse de grande pureté. Informations Chimie, 235, 163-166.

Langelin, H.R., Delannoy, A., Nicole, J. and Hennion, J. (1984) Préparation industrielle sélective des trois variétés cristallines du carbonate de calcium de synthèse. Informations Chimie, 252/253, 135-138.

Liendo, F., Arduino, M., Deorsola, F.A. and Bensaid, S. (2022) Factors controlling and influencing polymorphism, morphology and size of calcium carbonate synthesized through the carbonation route: A review. Powder Technology, 398, 117050.

Lin, Y., Chen, H., Chan, C.-M. and Wu, J. (2010) The toughening mechanism of polypropylene/calcium carbonate nanocomposites. Polymer, 51, 3277-3284.

Linke, W.F. and Seidell, A. (1958) Solubilities: Inorganic and metal-organic compounds. Fourth edition, Volume 1, pp. 1487, D. Van Nostrand Company, Inc., Princeton, New Jersey.

Mallick, P.K. (2007) Fiber-reinforced composites: Materials, manufacturing, and design, Third edition, pp. 619, CRC Press, Boca Raton.

Mao, Y., Yang, X. and Van Gerven, T. (2023) Amine-assisted simultaneous CO_2 absorption and mineral carbonation: Effect of different categories of amines. Environmental Science and Technology, 57, 10816-10827.

Massaro, F.R., Bruno, M. and Rubbo, M. (2014) Surface structure, morphology and (110) twin of aragonite. CrystEngComm, 16, 627-635.

Matsumoto, M., Fukunaga, T. and Onoe, K. (2010) Polymorph control of calcium carbonate by reactive crystallization using microbubble technique. Chemical Engineering Research and Design, 88, 1624-1630.

Moritomi, S., Watanabe, T. and Kanzaki, S. (2010) Polypropylene Compounds for Automotive Applications. R&D Reports "SUMITOMO KAGAKU", I, 1-16.

Murakami, K., Tanaka, H., Matsunaga, S., Hirakawa, M., et al. (1977) To provide a method for manufacturing aragonite type columnar calcium carbonate. Japan Patent, JP-1057431.

Nye, J.F. (1957) Physical properties of crystals. Their representation by tensors and matrices. pp. 322, Oxford University Press, London.

Ota, Y., Gotou, N., Motoyama, I., Iwashita, T. and Nomura, K. (1986) Production of acicular calcium carbonate particle. Japan Patent, JP-S61-120412.

Ota, Y., Inui, S. and Iwashita, T. (1991) Method forming acicular calcium carbonate particle. Japan Patent, JP-H05-221633.

Ota, Y., Inui, S., Iwashita, T., Kasuga, T. and Abe, Y. (1995) Preparation of Aragonite Whiskers. Journal of the American Ceramic Society, 78, 1983-1984.

Park, W.K., Ko, S.J., Lee, S.W., Cho, K.H., et al. (2008) Effects of magnesium chloride and organic additives on the synthesis of aragonite precipitated calcium carbonate. Journal of Crystal Growth, 310, 2593-2601.

Parkhurst, D.L. and Appelo, C.A.J. (2013) Description of input and examples for PHREEQC version 3: A computer program for speciation, batch-reaction, one-dimensional transport, and inverse geochemical calculations: U.S. Geological Survey Techniques and Methods, book 6, chap. A43, pp. 497, available only at https://pubs.usgs.gov/tm/06/a43/, Last accessed 23 January 2025.

Ramakrishna, C., Thenepalli, T. and Ahn, J.W. (2017) A brief review of aragonite precipitated calcium carbonate (PCC) synthesis methods and its applications-. Korean Chemical Engineering Research, 55, 443-455.

Reddy, M.M. and Nancollas, G.H. (1976) The crystallization of calcium carbonate IV. The effect of magnesium, strontium and sulfate ions. Journal of Crystal Growth, 35, 33-38.

Rivera, R.M. and Van Gerven, T. (2020) Production of calcium carbonate with different morphology by simultaneous CO_2 capture and mineralisation. Journal of CO_2 Utilization, 41, 101241.

Sakaguchi, H., Eguchi, K., Oda, T. and Nanri, Y. (2021) Method for producing calcium carbonate. Japan Patent, JP-7089311.

Sakaguchi, H., Oguni, S., Kita, K. and Nanri, Y. (2022) Method of producing calcium carbonate. Japan Patent, JP-7382091.

Sakuma, H., Andersson, M.P., Bechgaard, K. and Stipp, S.L.S. (2014) Surface tension alteration on calcite, induced by ion substitution. The Journal of Physical Chemistry C, 118, 3078-3087.

Santos, R.M., Ceulemans, P. and Van Gerven, T. (2012) Synthesis of pure aragonite by sonochemical mineral carbonation. Chemical Engineering Research and Design, 90, 715-725.

Sasaki, K., Hongo, M. and Tsunekawa, M. (1998a) Synthesis of aragonite-type of calcium carbonate from calcined scallop shell (2nd report) - With carbonates of aragonite-structure as seeds -. Shigen-to-Sozai, 114, 709-713.

Sasaki, K., Hongo, M. and Tsunekawa, M. (1998b) Synthesis of aragonite-type of calcium carbonate from calcined scallop shell (3rd report). Shigen-to-Sozai, 114, 715-720.

Sekkal, W. and Zaoui, A. (2013) Nanoscale analysis of the morphology and surface stability of calcium carbonate polymorphs. Scientific Reports, 3, 1587.

Shen, P., Jiang, Y., Zhang, Y., Liu, S., et al. (2023) Production of aragonite whiskers by carbonation of fine recycled concrete wastes: An alternative pathway for efficient CO_2 sequestration. Renewable and Sustainable Energy Reviews, 173, 113079.

Shibata, H., Takiyama, S. and Fujiwara, T. (1991) To provide a method for manufacturing aragonite crystal carbonate having a large particle size and the acicular shape. Japan Patent, JP-2787622.

Speer, J.A. (1983) Crystal chemistry and phase relations of orthorhombic carbonates. Reviews in Mineralogy and Geochemistry, 11, 145-190.

Sun, W., Jayaraman, S., Chen, W., Persson, K.A. and Ceder, G. (2015) Nucleation of metastable aragonite $CaCO_3$ in seawater. Proceedings of the National Academy of Sciences of the United States of America, 112, 3199-3204.

Tanaka, H., Horiuchi, H. and Ohkubo, T. (1988) Synthesis of whisker like aragonite $CaCO_3$. Gypsum and Lime, 216, 314-321.

U.S. Environmental Protection Agency (1998) MINTEQA2/PRODEFA2, A geochemical assessment model for environmental systems: User manual supplement for version 4.0. Athens, Georgia, National Exposure Research Laboratory, Ecosystems Research Division, pp. 76, Revised September 1999.

Voigt, W. (1890) Bestimmung der Elasticitätsconstanten für Kalkspath. Unter Benutzung der Biegungsbeobachtungen von G. Baumgarten. Annalen Der Physik, 275, 412-431.

Voigt, W. (1907) Bestimmung der Elastizitätskonstanten von Aragonit. Annalen Der Physik, 329, 290-304.

Vučak, M., Perić, J. and Krstulović, R. (1997) Precipitation of calcium carbonate in a calcium nitrate and monoethanolamine solution. Powder Technology, 91, 69-74.

Wakashima, K. (1976) Macroscopic mechanical properties of composite materials Part II. Elastic moduli and thermal expansion

coefficients. Journal of the Japan Society for Composite Materials, 2, 161–167.

Wang, M., Zou, H.K., Shao, L. and Chen, J.F. (2004) Controlling factors and mechanism of preparing needlelike $CaCO_3$ under high-gravity environment. Powder Technology, 142, 166–174.

Weber, S. (2011) JCrystal (Version 1.0.5). JCrystalSoft. Retrieved from http://www.jcrystal.com/, Last accessed 23 January 2025.

Woodall, C.M., McQueen, N., Pilorgé, H. and Wilcox, J. (2019) Utilization of mineral carbonation products: current state and potential. Greenhouse Gases: Science and Technology, 9, 1096–1113.

Wulff, G. (1901) XXV. Zur frage der geschwindigkeit des wachsthums und der auflösung der krystallflächen. Zeitschrift Für Kristallographie - Crystalline Materials, 34, 449–530.

Zhong, D., Zhang, W., Zhang, S., Hou, G. and Lu, B. (2024a) Preparation of aragonite whisker-rich materials by wet carbonation of magnesium slag: A sustainable approach for CO_2 sequestration and reinforced cement. Construction and Building Materials, 418, 135429.

Zhong, S., Yin, Y., Liang, X. and Deng, Q. (2024b) Aragonite and its composites: Preparations, properties and applications. European Journal of Inorganic Chemistry, 27, e202300733.

Zhou, G.-T., Yu, J.C., Wang, X.-C. and Zhang, L.-Z. (2004) Sonochemical synthesis of aragonite-type calcium carbonate with different morphologies. New Journal of Chemistry, 28, 1027–1031.

Manuscript received August 19, 2024
Manuscript accepted January 25, 2025
Advance online publication February 4, 2025
Released online publication February 26, 2025
Manuscript handled by Takaya Nagai